



HAL
open science

Getting simultaneous red and near infrared bands from a single digital camera for plant monitoring applications

Gilles Rabatel, N. Gorretta, S. Labbé

► To cite this version:

Gilles Rabatel, N. Gorretta, S. Labbé. Getting simultaneous red and near infrared bands from a single digital camera for plant monitoring applications. CIGR-Ageng 2012. International Conference on Agricultural Engineering, Jul 2012, Valencia, Spain. 6 p. hal-00777950

HAL Id: hal-00777950

<https://hal.science/hal-00777950>

Submitted on 18 Jan 2013

HAL is a multi-disciplinary open access archive for the deposit and dissemination of scientific research documents, whether they are published or not. The documents may come from teaching and research institutions in France or abroad, or from public or private research centers.

L'archive ouverte pluridisciplinaire **HAL**, est destinée au dépôt et à la diffusion de documents scientifiques de niveau recherche, publiés ou non, émanant des établissements d'enseignement et de recherche français ou étrangers, des laboratoires publics ou privés.

Getting simultaneous red and near infrared bands from a single digital camera for plant monitoring applications

Gilles Rabatel^{1*}, Nathalie Gorretta¹, Sylvain Labbé²

¹*Irstea, UMR ITAP, 361 rue Jean-François Breton, F-34196 Montpellier, France*

²*Irstea, UMR TETIS, 500 rue Jean-François Breton, F-34093 Montpellier, France*

**Corresponding author. E-mail: gilles.rabatel@irstea.fr*

Abstract

Multispectral images including red and near-infrared bands have proved their efficiency for vegetation-soil discrimination and agricultural monitoring in remote sensing applications. But they remain rarely used in ground and UAV imagery, due to a limited availability of adequate 2D imaging devices. In this paper, we propose and evaluate an original solution to obtain simultaneously the near-infrared and red bands from a standard RGB camera, after having removed the near-infrared blocking filter inside. First, the theoretical approach is described, as well as simulated results on a set of soil and vegetation luminance spectra with two different still cameras (Canon 500D and Sigma SD14). Then examples of images obtained in real field conditions are given, and compared with standard colour image acquisition for pixel-based plant/soil discrimination, using an automatic thresholding method. It appears that in most cases our new acquisition procedure brings a significative improvement, opening new opportunities for crop monitoring applications.

Keywords: multispectral sensor, near-infrared band, NDVI

1. Introduction

The Normalized Difference Vegetation Index, or NDVI, introduced in the early seventies by Rouse et al (1973), remains today a very popular tool in the remote sensing community dealing with agricultural monitoring. This is mainly due to its remarkable ability to discriminate vegetation from other material in multispectral satellite images.

Green vegetation is characterized by a high reflectance in the near-infrared domain (typically 50 to 80%), which contrasts with a very low reflectance in the red wavelengths, due to chlorophyll absorption. Let us call R and NIR the digital counts obtained through the red and the near infrared bands of a multispectral sensor. The NDVI, expressed as:

$$\text{NDVI} = (\text{NIR}-\text{R})/(\text{NIR}+\text{R}) \quad (1)$$

is a scalar value in the range [-1, 1]. The higher is this value, the higher is the probability that it corresponds to green vegetation. By extension, numerous attempts have been made to directly link NDVI or other derived indexes based on R and NIR to agronomical indices such as biomass and LAI or Leaf Area Index (Jindong et al, 2007).

The popularity of NDVI in remote sensing has been widely supported by the availability of R and NIR channels on most satellite line-scanning sensors (Landsat, SPOT, etc.). Unfortunately, it is not the case for crop monitoring applications at a lower spatial scale: most vision systems embedded on ground vehicles or UAV (Unmanned Aerial Vehicle), which require 2D sensors, are based on standard colour cameras, leading to robustness issues in vegetation detection.

To face this situation, some camera end users requiring a near infrared channel have developed alternative solutions around standard RGB cameras, taking benefit of an "undesirable" property of their silicon sensing array: because the colour filters in the Bayer matrix have a filtering action limited to the visible domain, the camera manufacturers are constrained to add a near-infrared blocking filter to match natural colorimetry requirements.

By removing this additional filter, we obtain a “modified” camera sensitive to near infrared wavelengths. A first possibility to get separate R and NIR bands is thus to use simultaneously a standard and a modified colour camera, the second one being equipped with a near infrared pass-band filter. However, important issues arise concerning the pixel alignment of the two images obtained (Lebourgeois et al, 2008).

Another interesting approach is to use a single modified camera, and to recover the red and near infrared bands as specific linear combinations of the three raw channels, provided an adequate filter is settled in front of the camera lens. The theoretical base of this approach has been detailed by Rabatel et al (2011). In the present paper, we will just recall its main results, and then emphasize on the results obtained in real field conditions.

For this purpose, various aerial images of field crop have been acquired, using both modified and standard still cameras, and their ability to discriminate between soil and crop have been compared.

2. Material and methods

2.1. Red and near infrared recovering from a single camera

Let us consider a three-channels camera, where the channels are characterized by their respective spectral sensitivities $c_1(\lambda)$, $c_2(\lambda)$, $c_3(\lambda)$, and a virtual channel sensitivity $s(\lambda)$ expressed as their linear combination : $s(\lambda) = a_1 \cdot c_1(\lambda) + a_2 \cdot c_2(\lambda) + a_3 \cdot c_3(\lambda)$. $s(\lambda)$ can be easily simulated from the camera, the digital count for a given pixel being equal to:

$$S = a_1 \cdot C_1 + a_2 \cdot C_2 + a_3 \cdot C_3 \quad (2)$$

where C_1 , C_2 , C_3 are the raw digital counts for this pixel. In that sense, $c_1(\lambda)$, $c_2(\lambda)$, $c_3(\lambda)$ build a 3D subspace of the general spectral space (with infinite dimension). Every possible simulated sensitivities are contained in this 3D subspace.

Now let us consider a desired virtual sensitivity $v(\lambda)$ (i.e. near infrared band). In the general case, $v(\lambda)$ will not be included in the subspace generated by $(c_1(\lambda), c_2(\lambda), c_3(\lambda))$, and the best approximation will be its projection $P(v)$ on this subspace (Fig. 1).

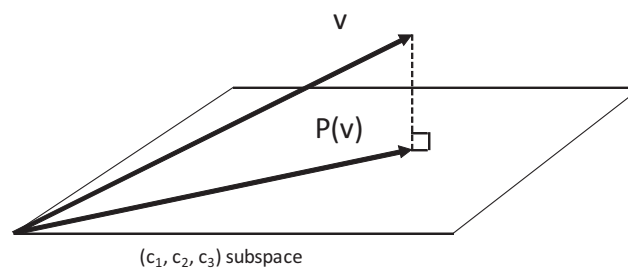


FIGURE 1: Approximation of a desired spectral sensitivity by projection

The quality of the approximation can be evaluated by the angle between the vectors v and $P(v)$, known in spectrometry as Spectral Angle Mapper or SAM (Yuhas et al, 1992).

Obviously, a standard RGB camera will allow recovering properly the red band (it has been designed for it) but not a near-infrared one, because the corresponding wavelengths (or dimensions) have been removed. What about a modified camera with no blocking filter ?

The approach involved here consists in searching for the best possible approximation for both red and near infrared bands, using an additional filter in order to modify the $c_1(\lambda)$, $c_2(\lambda)$, $c_3(\lambda)$ sensitivities, and thus the 3D projection sub-space. For technical reasons, only low-pass filters (cutting the short wavelengths) have been considered.

This study has been led with two high-level SLR (Single lens Reflex) cameras: Canon 500D (Canon, Tokyo, Japan) and Sigma SD14 (Sigma, Kawasaki, Japan), this last one having the particularity of being built around a 3-layered CCD sensor, instead of using a traditional matrix of microfilters. For both cameras, the near infrared blocking filter has been removed, and the resulting sensitivity curves $c_1(\lambda)$, $c_2(\lambda)$, $c_3(\lambda)$ have been measured in laboratory using the tunable monochromatic light source of a laboratory spectrometer (V-570, Jasco Inc, Easton, USA). Projections of standard Landsat red and near infrared bands have then been simulated for various low-pass filter cutting wavelengths using Matlab 7 (The MathWorks, Natick, MA, USA). For each cutting wavelength, the quality of the projections Q has been computed as the sum of SAM (in radian units):

$$Q = \text{SAM}_R + \text{SAM}_{\text{NIR}} = \text{SAM}(r(\lambda), P(r(\lambda))) + \text{SAM}(\text{nir}(\lambda), P(\text{nir}(\lambda))) \quad (3)$$

where $r(\lambda)$ and $\text{nir}(\lambda)$ are respectively the targeted red and near infrared sensitivities.

Finally, NDVI values have been computed for a set of vegetation and soil luminance spectra, and compared with NDVI issued from standard red and near infrared bands. These spectra were issued from hyperspectral images of wheat durum acquired in experimental fields (INRA, Domaine de Melgueil, France) in march 2011, using a Hypspec VNIR-1600 camera (Norsk Elektro Optikk, Norway).

2.2. Field crop image acquisition

According to results of the study above, various aerial images have been acquired using modified cameras (no infrared blocking filter) equipped with a Rot R8 (25 A) glass filter (Hama GmbH & Co, Monheim, Germany) in front of the lens. Depending on their availability, either a Canon 500D or a Canon 350D was used. Images were acquired by a private company (AvionJaune, Montferrier, France) using planes or Unmanned Aerial Vehicles (UAV), depending on the flight altitude.

For comparison purpose, the same aerial scenes have also been acquired using standard RGB cameras. In order to illustrate the plant/soil discrimination ability in both cases, the following procedure has been followed:

- for images acquired with the modified cameras, NDVI values have been computed using the R and NIR digital counts obtained from the procedure described in 2.1.
- for standard RGB images, the Excessive Green Index $\text{EGI} = 2G - R - B$ as well as its normalized version $\text{NEG} = \text{EGI}/(R+V+B)$ (Woebbecke et al, 1995) have been computed.
- NDVI, EGI and NEG images have then been computed by scaling the corresponding index values in the range 0-255, and thresholded according to their grey level histogram. For this purpose, we used the Otsu method (Otsu, 1979), which minimises the ratio between inter-class inertia and total inertia for the two classes issued from thresholding. This ratio, known as Wilk's lambda (Λ_w) in multivariate analysis, gives an indication on the thresholding quality and robustness.

In the following examples, NEG results will not be presented, because their Λ_w values were always lower than those obtained with EGI.

3. Results and discussion

3.1. Red and near infrared band projections

Fig. 2 shows the quality Q , as expressed in equation (3), of red and near infrared band projections for Canon 500D and Sigma SD14 cameras when varying the long-pass filter cutting wavelength.

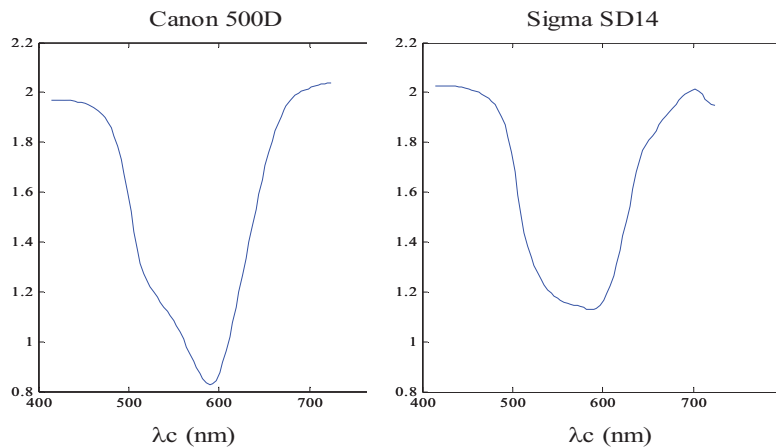


FIGURE 2: Red and near-infrared projection quality (in radians) as a function of the cutting wavelength

It appears that in both cases, the optimal projection is obtained for a cutting wavelength of about 600 nm, which corresponds to a red low pass filter. However, the best result is obtained with the Canon camera. For this reason, further studies will be limited to this type of camera, equipped with a photographic filter Hama Rot R8 (25 Å), cutting wavelengths below 600 nm. The corresponding red and near-infrared projections are expressed as:

$$P(r(\lambda)) = 0.0968 * c_1(\lambda) - 0.1722 * c_2(\lambda) + 0.0842 * c_3(\lambda) \quad (4)$$

$$P(nir(\lambda)) = -0.0455 * c_1(\lambda) + 0.0010 * c_2(\lambda) + 0.2605 * c_3(\lambda) \quad (5)$$

Fig. 3 shows the shape of these projections, as well as the corresponding NDVI values computed on our set of plant and soil spectra.

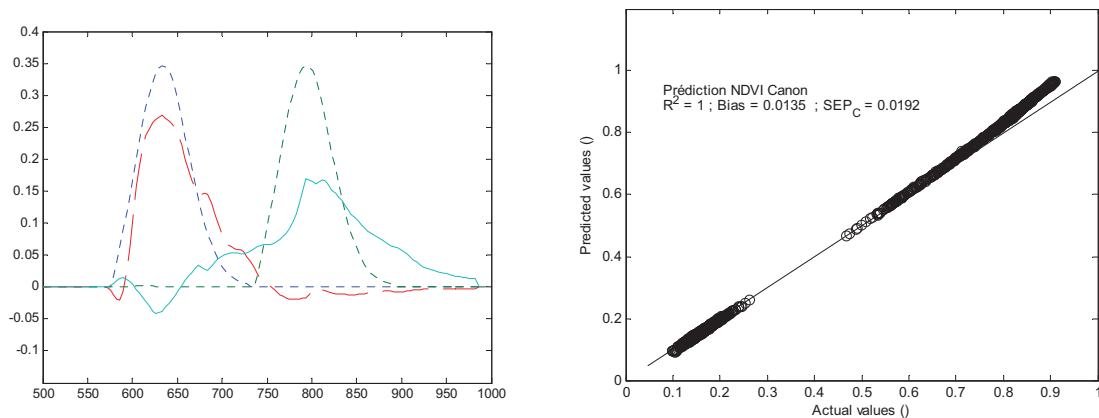


FIGURE 3: **left:** red and near-infrared projections $P(r(\lambda))$ and $P(nir(\lambda))$ using the Rot R8 filter (in dot lines: targeted sensitivities $r(\lambda)$ and $nir(\lambda)$). **right:** NDVI values computed with $r(\lambda)$, $nir(\lambda)$ (abscissa) and $P(r(\lambda))$, $P(nir(\lambda))$ (ordinate) on a set of soil and plant spectra

3.2. Field crop image acquisition

Fig.4 illustrates the various stages of NDVI computation using a single modified Canon 350D camera, as well as standard color acquisition for comparison. Images have been acquired in March 2012 on a wheat parcel (INRA, Mauguio, France) through two separate UAV flights. The flight altitude was about 30 m, and the spatial resolution was 1 cm. Only image portions are represented here.

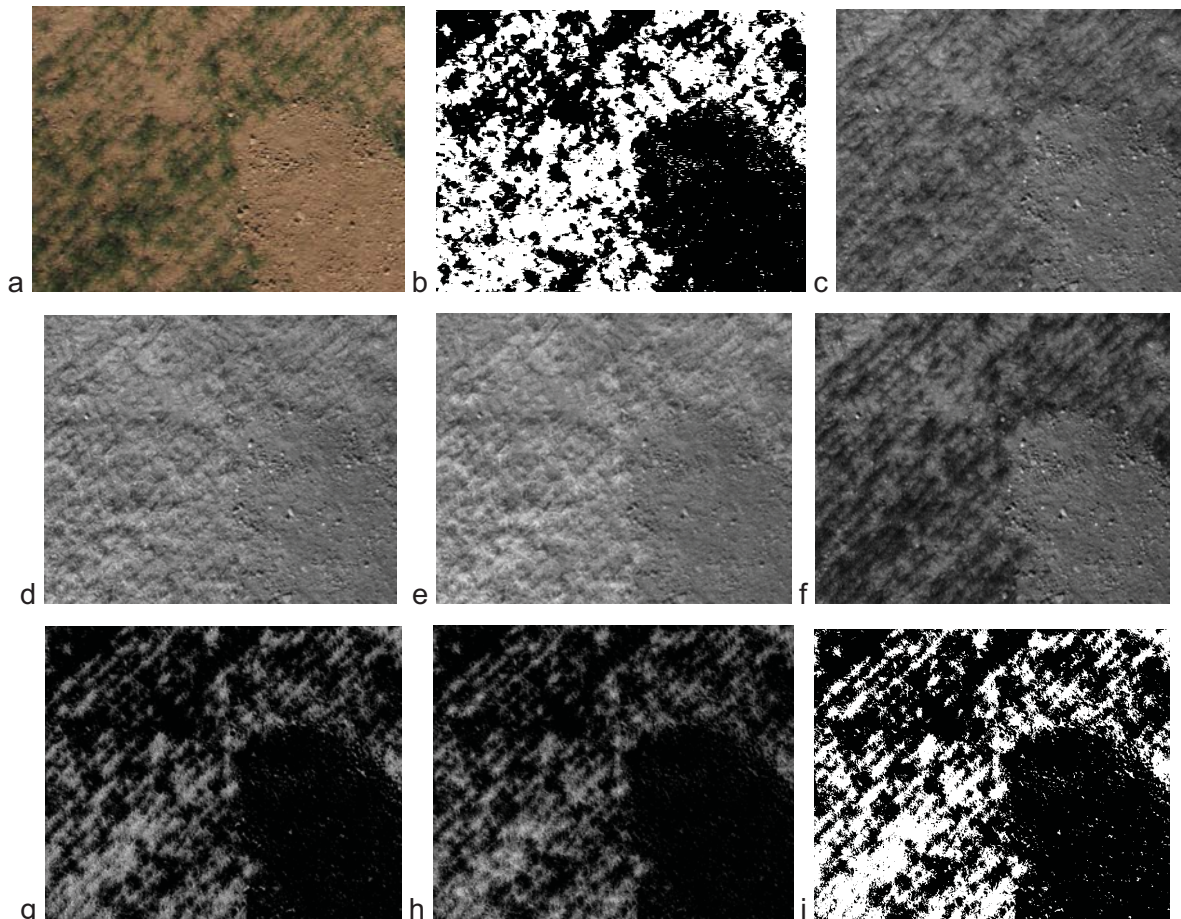


FIGURE 4: Details of image acquisition and NDVI computation on a wheat parcel
a: color image; **b**: EGI thresholding ($\Lambda_w=0.7054$); **c,d,e** : raw channels C1, C2, C3 of the modified camera; **f,g**: R and NIR bands issued from C1,C2,C3; **h**: NDVI obtained from R and NIR; **i**: NDVI thresholding ($\Lambda_w=0.8050$) (*bare soil zone: moisture sensor implementations*)

The better quality of NDVI thresholding compared to EGI thresholding is confirmed by the Wilks lambda values (resp 0.80 and 0.70). Also, we can notice that equations (5) and (6), determined from Canon 500D characteristics, are still usable with the Canon 350 D.

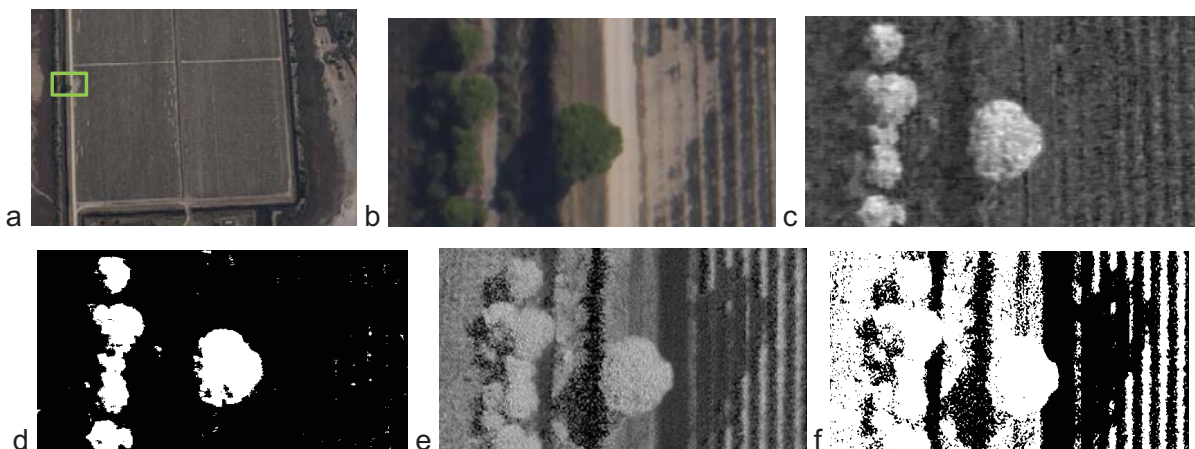


FIGURE 5: EGI and NDVI computation on a vine parcel
a,b: color image (full scale and detail); **c,d**: EGI computing and thresholding ($\Lambda_w=0.7333$);
e,f : modified camera NDVI computing and thresholding ($\Lambda_w = 0.70$)

Fig.5 shows a particular case including various types of vegetation. The corresponding images (standard and modified Canon 500D cameras, one flight for each) have been acquired in a vineyard area (Camargue, south of France) in September 2011, with a flight altitude of 1000 m and a 50 mm lens (spatial resolution ~ 10 cm).

According to images and Wilks lambda values, the EG index gives a better thresholding result. However, only the trees are discriminated from the soil. The vine rows (dark green) are not detected. In that sense, NDVI is more robust for plant detection.

4. Conclusion

We have shown in this paper that NIR and R bands can be issued from a single standard digital RGB still camera, by replacing the internal near-infrared blocking filter by an off-the-shelf low-pass filter set in front of the lens. Though the resulting red and near-infrared sensitivities do not match exactly the standard curves $r(\lambda)$ and $nir(\lambda)$, they provide satisfactory NDVI values for plant and soil, and thus bring more robustness in plant-soil discrimination, compared to standard color images.

These results are particularly interesting for in-field or low altitude imaging applications, which are presently mainly limited to standard color acquisition devices. In that sense, they open new possibilities in terms of high-resolution imaging for crop monitoring.

Reference list

Jindong, W., Dong, W. & Bauer M.E. (2007). Assessing broadband vegetation indices and QuickBird data in estimating leaf area index of corn and potato canopies. *Field crops research*, 102(1), 33-42.

Lebourgeois, V., Bégué, A., Labbé, S., Mallavan, B., Prévot, L. & Roux B. (2008). Can Commercial Digital Cameras Be Used as Multispectral Sensors? A Crop Monitoring Test, *Sensors*, 8(11), 7300-7322.

Otsu, N. (1979). A threshold selection method from gray-level histograms, *IEEE Transactions on Systems, Man and Cybernetics*, Vol. 9, No. 1, 62-66.

Rabatel, G., Gorretta, N. & Labbé, S (2011). Getting NDVI Spectral Bands from a Single Standard RGB Digital Camera: A Methodological Approach, *CAEPIA 2011, Lecture Notes in Artificial Intelligence*, 7023, 333–342/

Rouse, J. W., Haas, R. H., Schell, J. A. & Deering D. W. (1973). Monitoring vegetation systems in the great plains with ERTS, *Proceedings of the 3rd ERTS Symposium*, Vol. 1, 309-317.

Woebbecke, D.M., Meyer, G.E., Von Bargen, K. & Mortensen D.A. (1995). Color indices for weed identification under various soil, residue, and lighting conditions. *Transactions of the ASAE*, Vol. 38, Nr. 1, 259-269.

Yuhas, R.H., Goetz, A.F.H. & Boardman J.W. (1992). Discrimination among semi-arid landscape endmembers using the spectral angle mapper (SAM) algorithm, *Summaries of 3rd Annual JPL Airborne Geoscience Workshop*, JPL Publication 92-14, vol.1, 147-149.

Acknowledgements

The research leading to these results has received funding from the European Union's Seventh Framework Programme [FP7/2007-2013] under grant agreement n°245986.

We acknowledge L'avion jaune (<http://www.lavionjaune.fr/>) for having provided the modified cameras and made the aerial image acquisitions.